Changes in white matter in mice resulting from low-frequency brain stimulation

Denise M. Piscopo[a], Aldis P. Weible[b], Mary K. Rothbart[c], Michael I. Posner[b,c,1], and Cristopher M. Niell[a,b]

[a]Department of Biology, University of Oregon, Eugene, OR 97403; [b]Institute of Neuroscience, University of Oregon, Eugene, OR 97403; and [c]Department of Psychology, University of Oregon, Eugene, OR 97403

Contributed by Michael I. Posner, May 15, 2018 (sent for review February 6, 2018; reviewed by Richard J. Davidson and Ben Emery)

Recent reports have begun to elucidate mechanisms by which learning and experience produce white matter changes in the brain. We previously reported changes in white matter surrounding the anterior cingulate cortex in humans after 2–4 weeks of meditation training. We further found that low-frequency optogenetic stimulation of the anterior cingulate in mice increased time spent in the light in a light/dark box paradigm, suggesting decreased anxiety similar to what is observed following meditation training. Here, we investigated the impact of this stimulation at the cellular level. We found that laser stimulation in the range of 1–8 Hz results in changes to subcortical white matter projection fibers in the corpus callosum. Specifically, stimulation resulted in increased oligodendrocyte proliferation, accompanied by a decrease in the g-ratio within the corpus callosum underlying the anterior cingulate cortex. These results suggest that low-frequency stimulation can result in activity-dependent remodeling of myelin, giving rise to enhanced connectivity and altered behavior.

anterior cingulate cortex | electron microscopy | meditation | mouse | myelination

A variety of training methods have shown white matter change in humans using diffusion tensor imaging (DTI) (1, 2). These include training in working memory, juggling, and meditation (2, 3). Our human studies reported that 2–4 wk (30 min per day) of integrated body mind training (IBMT) resulted in white matter changes as measured by DTI around the anterior cingulate cortex (ACC) compared with a control group practicing relaxation (4, 5). IBMT, a form of mindfulness meditation, is associated with improvements in memory and attention and reductions in self-reported levels of negative affect (6).

We hypothesized (7) that the white matter changes might be due to increases in midfrontal theta oscillations (4–8 Hz) found in our study (8) and other research (9). Moreover, human studies have provided evidence that increases in theta current density are correlated with increased metabolism in the ACC (10). When the ACC receives theta stimulation that is in phase with stimulation of a lateral frontal area, there is an improvement in measures of executive function (11). Based on these findings, we wanted to explore the potential causal relationships between increased midfrontal theta and white matter change.

Depending on factors such as age and brain region, a given fraction of axons within white matter tracts are insulated by myelin. Myelination is thought to be critical for cognition because it is an effective mechanism for optimizing conduction velocity and coordinating spike-timing between distant brain regions (reviewed in refs. 12–14). It has been shown that adult-born oligodendrocytes contribute to remodeling of myelin and their activity can be modulated by both intrinsic and extrinsic factors (2). Specifically, studies in animal models show that proliferation, differentiation, and synthesis of myelin by oligodendrocyte progenitor cells (OPCs) are regulated by neural activity in both the developing and adult brain (13, 15–19). These results demonstrate that neuronal activity is sensed by oligodendrocytes and instructs the selective myelination of an active circuit.

There is mounting evidence from studies in rodents that natural experience can modulate myelination by oligodendrocytes in the adult, allowing the potential for improvement of neural circuit function. Learning a new skill can increase white matter and oligodendrocyte proliferation in regions of the brain engaged by the learned task (20–22). Conversely, social isolation can result in decreased myelination and impaired cognitive function (19, 23, 24). Furthermore, it has been shown that visual deprivation not only shortens the length of myelin internodes, but also results in reduced nerve conduction velocity in the optic nerve (25).

In an effort to elucidate the mechanisms involved in the regulation of myelination, a recent study using optogenetic stimulation of layer 5 pyramidal cells in the mouse motor cortex reported an increase in oligodendrocyte proliferation and differentiation within both the motor cortex and the subcortical projections of the corpus callosum (16). These changes were associated with myelin remodeling and improved behavioral performance. Another study (26) used an implanted electrode array to examine the effect of stimulation frequency (5, 25, or 300 Hz) on OPC proliferation and differentiation in the corpus callosum and effects were dependent upon the stimulation paradigm: 5-Hz stimulation showed the greatest effect on the differentiation of OPCs, whereas 25- and 300-Hz stimulation had the greatest effects on proliferation.

We previously reported the behavioral effects of rhythmic stimulation or suppression of ACC activity in mice (27). Using light-activated channels [both Channelrhodopsin-2 (ChR2) and Archaerhodopsin (Arch)], we drove periodic activation or inhibition of fast-spiking inhibitory interneurons at three different frequencies (1, 8, and 40 Hz) to increase or decrease the activity of ACC output neurons. We reported that mice receiving 1- and 8-Hz stimulation, which rhythmically increased ACC spike output, exhibited greater exploratory activity in the light area of a light/dark box compared

Significance

Meditation has been shown to modify brain connections. However, the cellular mechanisms by which this occurs are not known. We hypothesized that changes in white matter found following meditation may be due to increased rhythmicity observed in frontal areas in the cortex. The current study in mice tested this directly by rhythmically stimulating cells in the frontal midline. We found that such stimulation caused an increase in connectivity due to changes in the axons in the corpus callosum, which transmit impulses to and from the frontal midline. This work provides a plausible but not proven mechanism through which a mental activity such as meditation can improve brain connectivity.

Author contributions: D.M.P., A.P.W., M.K.R., M.I.P., and C.M.N. designed research; D.M.P. and A.P.W. performed research; D.M.P. analyzed data; and D.M.P., M.K.R., M.I.P., and C.M.N. wrote the paper.

Reviewers: R.J.D., University of Wisconsin–Madison; and B.E., Oregon Health & Science University.

The authors declare no conflict of interest.

[1]To whom correspondence should be addressed. Email: mposner@uoregon.edu.

Published online June 18, 2018.

with controls or mice receiving rhythmic suppression of cortical activity. Increased exploration in the light area of the light/dark box correlates inversely with anxiety (28). Therefore, our behavioral data were consistent with the reductions in anxiety reported by practitioners of IBMT (6) and interpreted as favoring the hypothesis that low-frequency stimulation could induce at least some of the behavioral benefits of meditation.

In the present study, using tissue obtained from the mice in our previous report (27), we sought to describe the effects of this stimulation paradigm at both the cellular and ultrastructural level. We hypothesized that low-frequency stimulation of the ACC in the theta range (4–8 Hz) could stimulate the proliferation and/or differentiation of oligodendrocytes and increase myelination as measured by electron microscopy (EM). Specifically, we focused on the genu of the corpus callosum because of its proximity to the site of laser stimulation and because it is one of the major tracts through which axons from the ACC project to the rest of the mammalian brain. Neurons sending projections through the corpus callosum relay sensory, motor, and other cognitive information between the two hemispheres. Furthermore, in our previous study (5) we found significant increases in fractional anisotropy (FA) in the body and genu of the corpus callosum following IBMT training.

First, we analyzed the effects of rhythmic stimulation and suppression on oligodendrocyte proliferation and differentiation. Subsequently, we used EM to assess changes in myelination and axon diameter following 1- and 8-Hz stimulation, the frequencies previously found to most effectively reduce anxiety-related behavior.

Results

Experimental Paradigm and Optogenetic Stimulation. To generate rhythmic spiking, we used two complementary optogenetic approaches. We bidirectionally manipulated parvalbumin-expressing (PV) inhibitory interneurons in the ACC using Arch and ChR2 to synchronize neuronal firing. In one experimental group, rhythmic decreases in spiking activity were induced in mice expressing ChR2 in PV cells (PV-ChR2) by delivering blue light pulses at 1, 8, or 40 Hz. In another experimental group, we used green light to generate rhythmic activity increases in mice expressing Arch (PV-Arch) in PV cells using the same frequencies and pulse durations. Fiber-implanted animals of each genotype that did not receive any light stimulation, as well as animals lacking optogenetic protein expression (PV-Cre), served as controls for injury or inflammation due to the implant surgery or heating generated by the optical fiber. Fig. 1*A* shows the location of the four bilaterally implanted optical fibers and recording electrodes used in these experiments. The local field potential and mean spiking activity for 8-Hz laser pulses in the PV-Arch and PV-ChR2 animals are shown in Fig. 1*B*.

Oligodendrocyte Proliferation and Differentiation Following Oscillatory Modulation of Neural Activity. In our previous study, we evaluated the behavioral effects of rhythmic manipulation of mouse ACC activity (27). Here, we investigate cellular responses within the corpus callosum of the same experimental animals. To characterize the effects of the various stimulation/suppression paradigms on oligodendrocyte proliferation or differentiation, we used the thymidine analog 5-ethynyl-2′-deoxyuridine (EdU) to label cells that had divided since the beginning of the stimulation period. Antibody staining against the transcription factor Olig2, a marker found in both OPCs and mature myelinating oligodendrocytes (OLs), was used to identify cells of the oligodendrocyte lineage.

Fig. 2*A* shows immunofluorescent staining for EdU and Olig2 in the corpus callosum near the site of stimulation. Fig. 2*B* displays the density of EdU^+Olig2^+ cells as a function of stimulation frequency and genotype, indicating cells of the oligodendrocyte lineage that have proliferated during the stimulation period. These data are also presented in Table 1. We first examined the density of EdU- and Olig2-stained cells as a function of experimental group and frequency of stimulation in a two-way ANOVA. We found a significant effect of experimental group [$F_{(2,\ 84)} = 3.6$; $P = 0.032$], frequency [$F_{(3,\ 84)} = 7$; $P = 0.0003$] and their interaction [$F_{(6,\ 84)} = 3.9$; $P = 0.0019$].

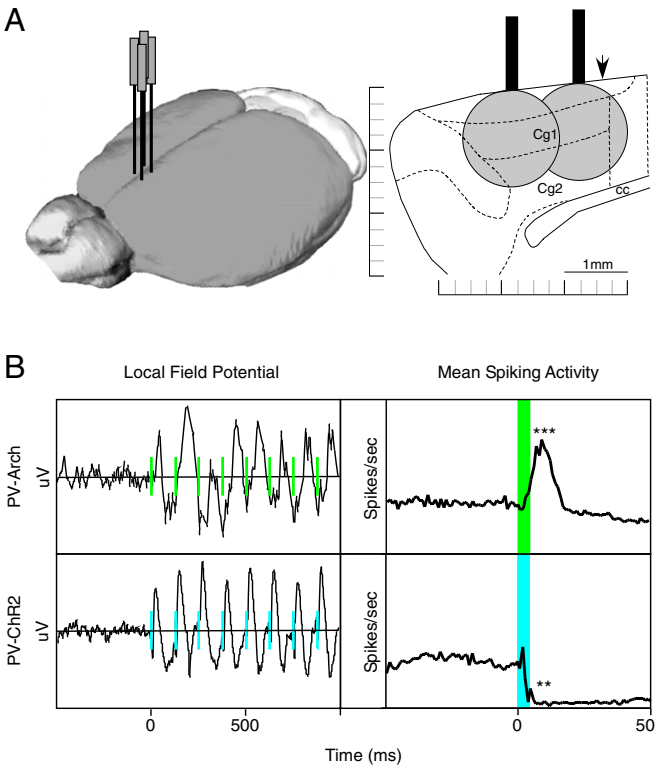

Fig. 1. Experimental design and effects of optogenetic stimulation. Light stimulation at 8 Hz produces a strong output signal at the same frequency. (*A*) Rhythmic manipulations of ACC activity was achieved by delivering light through a pair of fibers implanted in each hemisphere. Mice were implanted with two fibers overlying the ACC in each hemisphere (*Left*). Light intensities of 6.3 mW for 445-nm (ChR2) or 9.5 mW for 520-nm (Arch) resulted in an effective spread estimated to be 1.5 mm in diameter (*Right*). (*B*) Light delivery entrained local field potentials in both PV-Arch and PV-ChR2 mice at 1, 8, or 40 Hz (*Left*; 8 Hz shown). Light pulses elicited phase-locked increases in spiking activity in PV-Arch mice, and phase-locked decreases in spiking activity in PV-ChR2 mice. Light delivery in PV-PV mice not expressing either light-sensitive opsin produced no effect on spiking activity (27). cc, corpus callosum; cg1&2, anterior cingulate subdivisions; PV, parvalbumin. $^{**}P < 0.01$; $^{***}P < 0.001$.

A 1-Hz cortical stimulation in PV-Arch mice resulted in an increased density of EdU^+Olig2^+ cells compared with non-stimulated controls ($P = 0.0041$ by Tukey post hoc test). Notably, activating Arch in PV neurons at a 1-Hz rhythm resulted in more proliferating oligodendrocytes than activating ChR2 in PV neurons at any frequency. In fact, ChR2 activation appeared to decrease numbers of proliferating oligodendrocytes at all frequencies. We looked for signs of apoptotic cell death measured by cleaved caspase-3 labeling in brain sections stained at the end of the 4-wk stimulation period. Although we occasionally saw some labeled cells at the site of the fiber implant, we did not observe obvious differences between the groups, either by genetic background or laser-stimulation frequency. This supports the notion that neither stimulation nor suppression at these intensities and frequencies was harmful. To identify the fate of proliferating cells in the corpus callosum, we stained adjacent brain sections for CC1, a marker of mature oligodendrocytes (Fig. 2*C*). Cells that had divided since the beginning of the stimulation period, and had differentiated into mature oligodendrocytes capable of myelination, would thereby be labeled

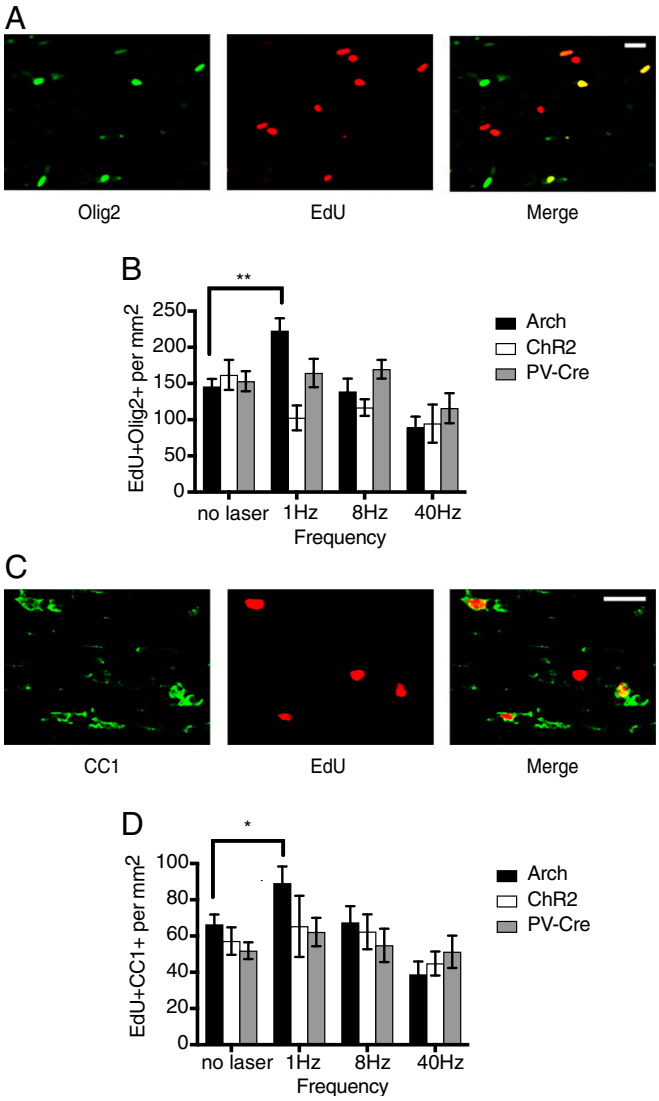

Fig. 2. PV-Arch 1-Hz stimulation promotes oligodendrocyte proliferation and differentiation. Effects on cells of the oligodendrocyte lineage to stimulation/inhibition of neuronal activity at different frequencies. (*A*) Confocal image (20×) of cells in the corpus callosum labeled with an Olig2 antibody to identify cells of the oligodendrocyte lineage (green). Cells that have proliferated during the 4-wk stimulation period are labeled with the thymidine analog EdU (red). Colocalization of EdU and Olig2 (yellow) identifies oligodendrocytes that have proliferated since the beginning of the stimulation protocol. (*B*) Graph of mean density of proliferating oligodendrocytes (EdU^+Olig2^+) as a function of frequency for each of the genotypes. (*C*) Image of cells labeled with CC1 antibody (green) which marks mature oligodendrocytes. EdU^+ cells are labeled red. Merge indicates EdU tagged mature oligodendrocytes. (*D*) Graph of mean density of mature oligodendrocytes (EdU^+CC1^+) generated over the stimulation period as a function of frequency for each of the genotypes. Error bars indicate SEM. (Scale bars, 20 μM.) $^*P < 0.05$; $^{**}P < 0.01$.

with both EdU and CC1. The results of the staining analyzed by experimental group and frequency are shown in Fig. 2*D*.

A two-way ANOVA yielded only an effect of stimulation condition [$F_{(3,\ 84)} = 4.3$; $P = 0.0073$]. A Tukey multiple-comparison analysis showed no significant increase in EdU^+CC1^+ cells following low-frequency stimulation overall, although a trend was seen in the 1-Hz group compared with nonstimulated controls (1 Hz: $P = 0.0785$; 8 Hz: $P = 0.9995$). The Tukey test estimates the variance using all of the genotypes and stimulation conditions. If we compare each stimulation condition separately to nonstimulated controls using unpaired *t* tests, we find that the 1-Hz group was significantly different from the nonstimulated control ($t = 2.2$, $P = 0.0348$). As with Olig2, the density of EdU^+CC1^+ cells for the PV-Arch 40-Hz group was below the nonstimulated controls. It is important to note that our assay would not have identified cells that were born before the stimulation period and were induced to differentiate by the stimulation.

Evaluation of Axon Fibers by EM. Based on the oligodendrocyte proliferation and differentiation results, we focused on low-frequency stimulation in the PV-Arch animals for examination of axon diameter and myelin thickness at the ultrastructural level by transmission electron microscopy (TEM). Imaging at 16,000× was performed on 10 PV-Arch mice that had undergone the same 4-wk stimulation protocol (Fig. 3*A*). Six animals were stimulated at either 1 or 8 Hz, and four were nonstimulated controls with fiber implants. Myelinated axons were visualized in the corpus callosum and in the anterior commissure as a control. Relative myelin thickness is calculated as the ratio of the axon caliber (diameter) to the fiber caliber (total diameter of axon plus its myelin sheath), also known as the g-ratio. The g-ratio was calculated for myelinated axons in each experimental group both in the corpus callosum and the anterior commissure (Fig. 3*B*). These data are also presented in Table 2.

In the corpus callosum, the average g-ratio was 0.75 ± 0.011 for the control group, similar to what has previously been reported in mice (16, 29), and 0.71 ± 0.005 for the stimulated groups. Using a one-way ANOVA to compare g-ratio values as a function of stimulation group (no laser control, 1 and 8 Hz) in each brain area (corpus callosum or anterior commissure), we found a significant effect of stimulation group for the corpus callosum ($F = 7.385$; $P = 0.0046$), but not the anterior commissure ($F = 2.65$, $P = 0.11$). Dunnett's multiple-comparisons test returned significant *P* values for both 1 Hz ($P = 0.0221$) and 8 Hz ($P = 0.0062$) compared with nonstimulated controls. Because there were only two mice in the 1-Hz group and four in the 8-Hz group, we combined the two into a low-frequency stimulated group. Comparing this stimulated group with the nonstimulated control also demonstrated a significant difference ($P = 0.0033$). The mean g-ratio within the control region (anterior commissure) for the nonstimulated (0.72 ± 0.0012) and stimulated groups (0.72 ± 0.0045) was not different.

Fig. 3*C* shows a scatter plot of g-ratio as a function of axon diameter for each of the three groups. The slope of the linear fit to the data gives an indication of the myelin thickness for a given axon caliber. The slope for the 1-Hz group (0.271) did not differ significantly from the 8-Hz group (0.276), therefore we calculated one slope for both stimulated groups. The difference between the slopes of the stimulated (0.274) and nonstimulated groups (0.229) is highly significant ($F = 7.12$, $P = 0.0008$).

A decrease in g-ratio could be accounted for by either an increase in myelin thickness or a decrease in axon caliber. Fig. 3 *D* and *E* show measures of myelin thickness and axon diameter separately. Comparing the low-frequency stimulated group to the nonstimulated group, there was a small increase in myelin thickness (0.16 ± 0.003 vs. 0.17 ± 0.002) (Fig. 3*D*) as well as a decrease in the fraction of large caliber axons (0.50 ± 0.03 vs. 0.45 ± 0.013) (Fig. 3 *E* and *F*). Although there appears to be a contribution of each factor to the change in g-ratio, neither factor alone reached statistical significance for the stimulated group compared with the no-laser control ($P = 0.0598$ for myelin thickness and $P = 0.1354$ for axon diameter). To test whether the reduced fraction of larger diameter axons following stimulation might reflect de novo myelination of small fibers that were unmyelinated before stimulation, we counted the number of myelinated vs. unmyelinated fibers of at least 100-nm diameter in the corpus callosum. No significant increase in de novo myelination was apparent in the stimulated group over the control in the percentage of myelinated axons [stimulated animals (54.8 ± 3.1%) vs. nonstimulated controls (55.9 ± 4.42%)].

Table 1. Oligodendrocyte proliferation and differentiation data

	No laser			1 Hz			8 Hz			40 Hz		
Olig2 or CC1	Mean	SEM	*n*	Mean	SEM	*n*	Mean	SEM	*n*	Mean	SEM	*n*
Olig2												
Arch	145.7	10.7	8	222.9	17.3	6	138.9	17.9	5	89.2	15.0	5
ChR2	161.9	20.7	3	102.5	17.2	3	116.7	11.5	3	94.6	26.4	3
PV	152.9	13.9	3	164.3	19.5	3	169.4	12.9	3	115.6	20.8	3
CC1												
Arch	66.4	5.5	8	89.1	9.3	6	67.5	9.0	5	38.8	7.2	5
ChR2	57.1	7.6	3	65.3	16.9	3	62.2	9.6	3	44.7	6.6	3
PV	51.9	4.6	3	62.2	7.8	3	54.8	9.2	3	51.3	8.9	3

Correlation of Myelination Data with Behavior. Previously, we presented data showing that low-frequency stimulation at 1 or 8 Hz increased the time animals spent exploring the illuminated half of the light-dark box. In Fig. 4, we show increased time spent in the light is correlated with a decrease in g-ratio calculated from the EM data. Given the small number of experimental animals, we used a nonparametric comparison of the g-ratio and the amount of time spent in the light (Kendall's τ of -0.501 and $P = 0.04$). It is clear that this relationship is driven by the higher g-ratios in the nonstimulated control group, rather than individual variability within the stimulated groups. Although the figure suggests that a reduction in g-ratio is related to reduced anxiety and greater exploration in poststimulation behavior, the largest effect is driven by whether the animals were stimulated or not.

Discussion

Our results can be summarized as follows: (*i*) Optogenetic stimulation of the mouse ACC in the range of 1–8 Hz results in changes to white matter in the corpus callosum. (*ii*) This low-frequency stimulation results in increased oligodendrocyte proliferation, accompanied by a decrease in the g-ratio within the corpus callosum underlying the ACC. (*iii*) These results suggest that low-frequency stimulation can result in activity-dependent remodeling of myelin, which could lead to enhanced connectivity and altered behavior. We discuss each of these points below.

Changes in Oligodendrocytes and Axonal Structure. We found a significant increase in EdU^+Olig2^+ oligodendrocytes following 1-Hz stimulation in the PV-Arch group in comparison with nonstimulated controls. However, the increase in EdU^+CC1^+ cells, indicating numbers of newly born oligodendrocytes that are mature and capable of myelination, was less robust. It is possible that this is due to the small number of mice involved in the critical conditions, but we also speculate on possible biological explanations for this result, some of which are outlined in Fig. 5. It is conceivable that different aspects of oligodendrocyte maturation are regulated by different factors, and 1-Hz stimulation specifically regulates those related to proliferation. Another possible explanation is that 1-Hz, and possibly 8-Hz stimulation could have effects on the myelinating activity of postmitotic oligodendrocytes, which would not have been labeled with EdU, and thus would not have been identified in our analysis. This alternative could account for why both 1- and 8-Hz stimulation were able to affect the g-ratio and why both also affect behavior. It is also possible that the oligodendrocyte precursors generated by 1-Hz stimulation might not have differentiated into mature myelinating oligodendrocytes. There is evidence that oligodendrocyte precursors can perform metabolic support functions for axons and help maintain homeostasis at synapses rather than becoming myelinating oligodendrocytes (30–34). Finally, oligodendrocyte proliferation could have been activated by inflammation or injury associated with the stimulation protocol (35–38). However, this explanation seems unlikely as: (*i*) we saw no evidence of apoptosis in the stimulated area at the time of euthanasia (39), (*ii*) no behavioral deficits were noted during any of the paradigms tested in our previous study, and (*iii*) the effects were seen specifically with the PV-Arch mice, while both PV-Arch and PV-ChR2 animals would have experienced localized heating of the tissue with light delivery.

Both axon diameter and myelin thickness contribute to neuronal conduction velocity (13, 14), and even small changes in either parameter can have a meaningful impact on transmission speed. The g-ratio is a quantitative measure of optimal axonal myelination and is calculated by dividing the axon diameter by the diameter of the fiber (axon plus myelin). We found that both 1- and 8-Hz stimulation of PV-Arch animals were essentially equivalent in producing a decrease in g-ratio relative to nonstimulated controls in the corpus callosum, which contains axons from the ACC, but not in the more distally located anterior commissure, which does not contain axons from the ACC. Nonstimulated control values for the corpus callosum and anterior commissure are in agreement with previously published values (16, 29, 40). Both 1- and 8-Hz stimulation resulted in a decreased g-ratio, although only 1-Hz stimulation appreciably increased oligodendrocyte proliferation. It is possible that 1-Hz stimulation drives oligodendrocytes to divide, whereas 8-Hz stimulation drives myelination. Although there is evidence that myelin remodeling can occur independently of OPC proliferation (41), it is unclear to what extent mature OLs can modulate their myelination (37, 38).

Changes in myelination or axon diameter alter the g-ratio and can result in a reduction of conduction velocity. Given that the theoretical value for the optimal g-ratio has been calculated to be 0.6 (40, 42), it would be interesting to examine changes in conduction velocity resulting from the observed reduction in g-ratio seen here. However, communication between brain regions does not depend specifically on the speed of transmission, but on the synchronization of inputs. Thus, optimal connectivity may not require optimal velocity. Unfortunately, we were unable to follow individual axons to determine which ones were directly affected by the optogenetic stimulation. Furthermore, in our experiments we were not able to examine potential changes in the pattern of myelination along the length of an axon. The length of myelinated segments and the spacing between them (internodes) are also factors that can contribute to changes in conduction velocity (43–45). Investigating the contribution of each of these factors to stimulation-induced changes in white matter should be topics for future study.

The reduction in g-ratio in our experiments appears to be due to a combination of both increased myelination and a reduction in myelinated axon caliber in stimulated mice compared with controls. One possibility is that that the stimulation protocol resulted in de novo myelination of small nonmyelinated fibers, which would shift the population to smaller diameters overall. However, we did not see a change in the overall percentage of myelinated fibers in the corpus callosum. There is evidence that axon diameters scale by firing frequency (46), suggesting that perhaps axons could not only increase diameter in response to firing rate, but could also decrease. However, we are not aware of similar studies describing a reduction in axon diameter with stimulation or learning.

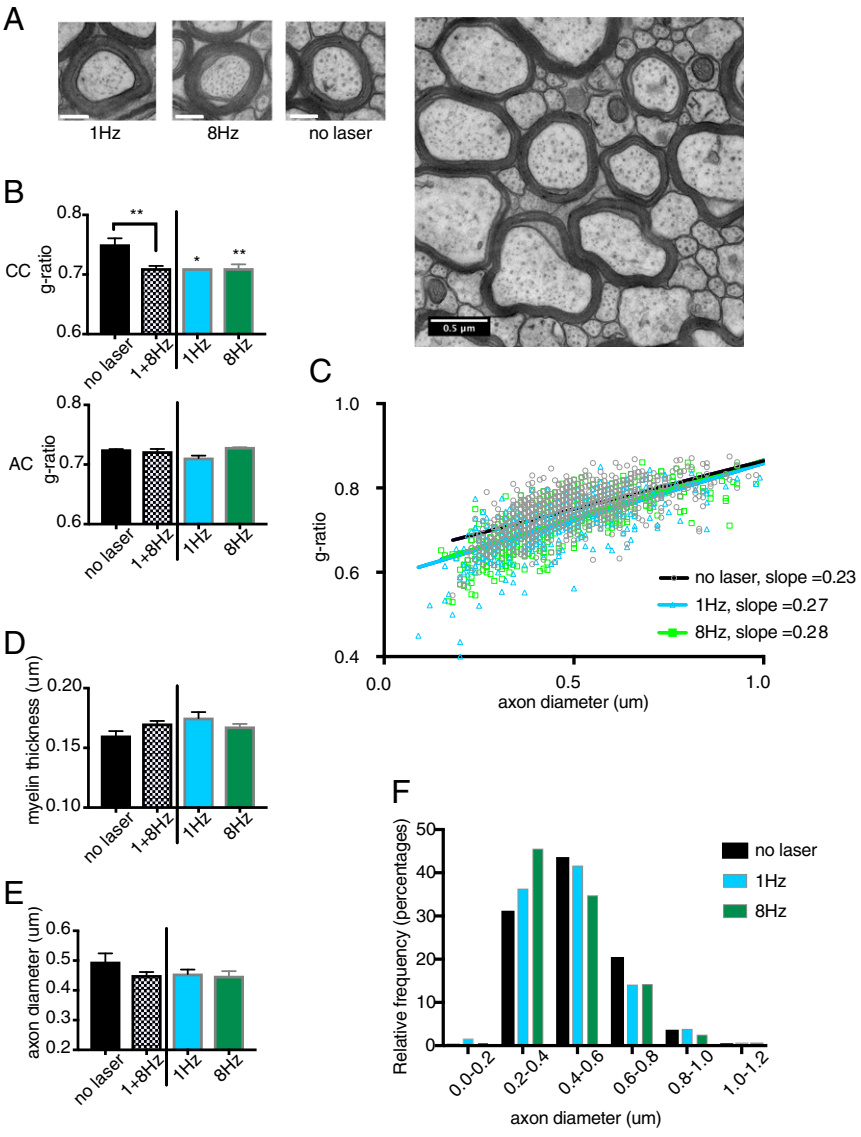

Fig. 3. Low-frequency stimulation reduces the g-ratio of axons in the corpus callosum. (*A*) Example images of individual axons for each condition. (Scale bar, 0.2 μM.) A representative electron micrograph used to assess g-ratio acquired with TEM at 16,000× magnification. (Scale bar, 0.5 μM.) (*B*) Quantification of mean g-ratio of axons in the corpus callosum vs. anterior commissure for nonstimulated and stimulated (1 and 8 Hz) PV-Arch groups. (*C*) Scatterplot of g-ratio versus axon diameter for stimulated and nonstimulated groups fit with a linear function. (*D*) Quantification of mean myelin thickness for myelinated axons in the corpus callosum. (*E*) Quantification of mean axon diameter for myelinated axons in the corpus callosum. (*F*) Frequency distribution of myelinated axons according to their diameters. Error bars indicate SEM. $*P < 0.05$; $**P < 0.01$.

Role of Stimulation Frequency. Our previous work showed that 2–4 wk of meditation training produced significant increases in FA in pathways surrounding the ACC in comparison with relaxation training controls (4, 5). The largest increases in FA were seen in the body and genu of the corpus callosum, superior corona radiata, and superior longitudinal fasciculus. The change in FA measured at 2 wk was due to a decrease in axial diffusivity, thought to represent axonal density increases (47). Measurement by DTI at 4 wk found that the increase in FA involved both radial diffusivity, sometimes thought to represent changes in myelin (48–50), as well as axial diffusivity. We speculated that the increase in FA might be due to a frontal theta rhythm (4–8 Hz), which is also increased following meditation training (8).

This work in humans was the impetus for our study in mice using the inhibitory network to rhythmically increase (PV-Arch) or decrease (PV-ChR2) firing rates across the cortical population. We found that only increases in activity in the ACC were associated with increased exploratory behavior (27), as well as maturation of oligodendrocytes and reduced myelin g-ratio (current study). However, our results are not entirely consistent with the hypothesis that theta rhythms are primarily responsible for the beneficial changes underlying IBMT. Exploratory behavior was increased most by 8-Hz stimulation, but overlap in EdU and Olig2 labeling was greater for 1-Hz stimulation. Furthermore, 1- and 8-Hz stimulation

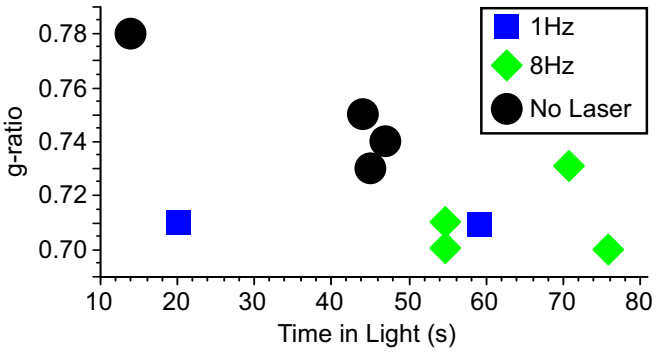

Fig. 4. The g-ratio is correlated to behavior after low-frequency rhythmic stimulation. Plot of relationship between time in light during a light/dark box paradigm as a behavioral parameter and g-ratio for the different stimulation conditions in PV-Arch mice.

Table 2. TEM myelination and axon caliber data

Condition	*n*	No. axons	G ratio		Axon diameter, μm		Fiber diameter, μm		Myelin thickness, μm		Percent myelinated, %	
			Mean	SEM	Mean	SEM	Mean	SEM	Mean	SEM	Mean	SD
Corpus callosum												
No laser	4	868	0.75	0.011	0.50	0.030	0.65	0.030	0.16	0.003	55.9	4.42
1 Hz	2	410	0.71	0.001*	0.45	0.028*	0.63	0.037*	0.17	0.009*	54.3	0.403
8 Hz	4	565	0.71	0.007	0.45	0.018	0.62	0.020	0.17	0.003	55.4	5.24
1 + 8 Hz	6	975	0.71	0.005	0.45	0.013	0.62	0.014	0.17	0.002	54.8	3.10
Anterior commissure												
No laser	3	292	0.72	0.001								
1 Hz	2	86	0.71	0.006*								
8 Hz	3	210	0.73	0.0003								

*Indicates SD due to small number.

were essentially equivalent in changing axon diameter and myelination at the ultrastructural level.

The prospect that different stimulation frequencies could underlie distinct changes at the ultrastructural, cellular, and behavioral levels warrants further investigation. Indeed, different stimulation frequencies are known to be effective for different aspects of behavior and physiology. Nagy et al. (26) demonstrated that electrical stimulation of activity at different frequencies in the corpus callosum had distinct effects, with low-frequency stimulation promoting oligodendrocyte differentiation and high-frequency stimulation driving proliferation. Activity-dependent regulation of oligodendrocyte maturation or activity could also vary depending on brain region, cell-type, frequency of stimulation, synchrony of firing with respect to other axons, duration of stimulation, or gender of the animal. There is still much work to be done to characterize how cells of the oligodendrocyte lineage respond to different patterns of neuronal activity.

Impact on Brain Function. The ACC is involved in high-level attentional control (51). We speculate that changes in white matter could allow better synchronization of conduction velocities between medial frontal areas and other limbic structures like the amygdala, and could thus underpin effects such as those seen with exploratory activity and anxiety in previous work (27, 52, 53). To test this idea, we compared the g-ratio from individual mice to their behavior in the light/dark box. Despite the small sample size, there is an inverse relationship between the g-ratio and time spent exploring the apparatus. This relationship is confounded by the stimulation protocol because stimulated mice have a lower g-ratio. However, the data support a potential link between our behavioral observations (27) and changes in the degree of connectivity.

Although the stimulated 1- and 8-Hz groups showed only about a 10% decrease in g-ratio and a small increase in myelination, this may have been sufficient to reduce anxiety and increase the time mice spent in the light. Increased FA found in our meditation

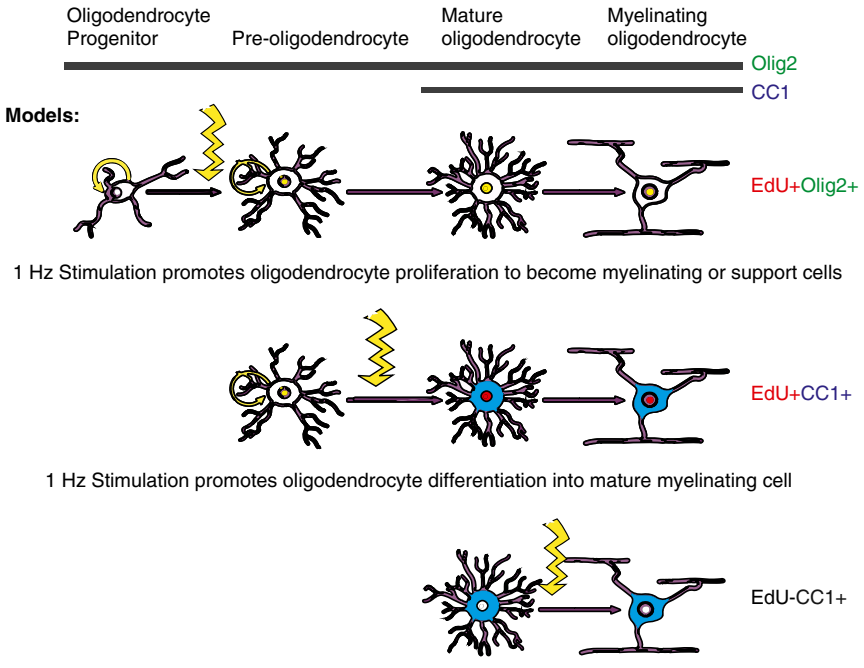

Fig. 5. Effect of neuronal activity on myelination. Model for potential mechanisms by which rhythmic stimulation could affect proliferation of OPCs, differentiation into OLs or synthesis of myelin (see *Discussion* for details). Colors and distribution represent mock immunohistochemistry staining (EdU = red, nuclear; Olig2 = green, nuclear; $EdU^{+}Olig2$ = yellow, nuclear; CC1 = blue, cytoplasmic). Illustration modified from ref. 58.

studies in pathways related to the ACC was about 10% above its initial value (5). These studies suggest that the changes in white matter due to experience could be similar in quality and magnitude in humans and mice.

There is evidence that rhythmic stimulation in the theta range delivered to frontal areas can modulate behavioral performance in humans. One recent study found that 6-Hz transcranial alternating current stimulation over midline and the lateral frontal cortex improved executive function when synchronized, and reduced executive function when desynchronized (11). Many researchers have reported improved learning and performance with direct current frontal stimulation (54), although these results are mixed (55). It is also possible that such stimulation works in whole or part through stimulating an intrinsic rhythm (56).

Based on the findings in mice, we speculate that inducing low-frequency rhythmic activity in humans over multiple sessions by ACC stimulation might be sufficient to alter connectivity and perhaps produce similar white matter changes found with meditation. Inducing such a rhythm less invasively in humans, whether by electrical stimulation, sensory stimulation, or neurofeedback, might work to change white matter in different brain areas and thus serve to improve functionality. The effectiveness of such stimulation might also be enhanced if accompanied by a task activating the same brain areas. If true, it might be possible to improve or restore white matter in any area of the brain for which appropriate electrodes and tasks could be designed. These ideas are preliminary, but they support the need for more research to understand the effects of brain stimulation on behavior and the underlying biological mechanisms.

Methods

All studies were conducted with approved protocols from the University of Oregon Institutional Animal Care and Use Committee, in compliance with National Institutes of Health guidelines for the care and use of experimental animals.

Mice. In the present study, we assessed the effects of rhythmic suppression or stimulation of cortical activity in mice expressing the light-gated ion channel ChR2 or the proton pump Arch in PV^+ inhibitory interneurons. Parents were homozygous for Pvalb-IRES-Cre (PV, 008069; The Jackson Laboratory), Rosa-CAG-LSL-ChR2(H134R)-EYFP-WPRE (ChR2, 012569; The Jackson Laboratory), or Rosa-CAG-LSL-Arch-GFP-WPRE (Arch, 012735; The Jackson Laboratory). Optogenetic suppression of the ACC was performed using offspring heterozygous for both PV and ChR2 (PV-ChR2). Optogenetic stimulation was performed using offspring heterozygous for both PV and Arch (PV-Arch). Mice homozygous for Pvalb-IRES-Cre (PV-PV) were utilized to control for nonspecific effects of pulsed light delivery. Data were collected from both male and female mice, aged 8–12 wk at the time of surgery. A total of 26 PV-Arch, 16 PV-ChR2, and 10 PV-PV mice were included in immunohistochemistry experiments. A total of 10 PV-Arch mice were included in EM work.

Surgery. To study the behavioral effects of rhythmic cortical activity manipulations, mice were implanted with a 2×2 array of 200-μm diameter optic fibers overlying each hemisphere of the ACC. To determine whether these phasic manipulations of cortical activity altered baseline power of intrinsic rhythms, identical arrays were modified to include a single Teflon-coated stainless steel local field potential recording electrode in each hemisphere between each pair of optic fibers. For recording single-neuron activity, a four-tetrode array with a single 200-μm optic fiber was implanted in the ACC. Mice were administered carprofen (5.0 mg/kg) postoperatively to minimize discomfort and allowed 7 d of postoperative recovery.

Stimulus Delivery. Mice from all three genetic backgrounds were randomly assigned to a 1-Hz (200 ms pulses), 8-Hz (5 ms pulses), 40-Hz (5 ms pulses), or no-laser condition. Mice were given 20 sessions of light pulses (30 min/d, 5 d/wk over 4 wk). For PV-Arch mice, 520-nm wavelength modules were set to 9.5 mW. For PV-ChR2 mice, 445-nm wavelength modules were set to 6.3 mW. These intensities were selected to produce an effective spread through a volume of tissue ~1.5 mm in diameter, thus restricting the direct effect predominantly to the ACC.

Immunohistochemistry. Mice were anesthetized with Euthasol and perfused first with phosphate buffer (PB, pH 7.4) containing heparin (10 units/mL; Sagent Pharmaceuticals) and then with 4% paraformaldehyde (PFA; Electron Microscopy Sciences, EMS) in 0.1 M PB. Brains were removed, immersed in fresh 4% PFA and stored at 4 °C overnight. Tissue was cryo-protected in 30% (wt/vol) sucrose in 0.1 M PB for 48 h. All brains were embedded in optimal cutting temperature compound and coronal cryo-sections (30-μm thickness) were collected into cryoprotectant medium [30% (wt/vol) sucrose, 1% (wt/vol) polyvinyl-pyrrolidone, 30% (vol/vol) ethylene glycol in 0.1 M PB] and stored at −20 °C before staining. Immunohistochemistry was performed on floating sections.

For immunolabeling, sections were washed with 0.1 M PB and permeabilized with blocking solution containing 0.3% Triton-X100 and 6% Normal Donkey serum (NDS; Sigma) before incubating overnight with rabbit anti-MBP (1:5,000; Abcam), mouse monoclonal CC1 (1:500; against adenomatous polyposis antigen; Calbiochem), or rabbit anti-OLIG2 (1:500; Millipore). Sections were washed three times with 0.1 M PB before adding AlexaFluor 657-conjugated anti-rabbit IgG or AlexaFluor 488-conjugated anti-mouse IgG (1:5,000; Invitrogen) in blocking solution. Floating sections were transferred onto gelatin-coated glass slides and mounted using Fluoromount-G (Southern Biotech). Sections were costained with rabbit anti-Caspase3 (1:500; Cell Signaling Technology) to quantify cell death.

EdU Labeling and Detection. EdU (Invitrogen) is a thymidine analog that is incorporated into the DNA of cells as they undergo DNA replication. EdU was administered to mice via the drinking water (0.2 mg/mL) that was available ad libitum and replaced every day. To determine the identity of newly born cells, 30-μm floating sections were first processed and stained as above to detect CC1 or Olig2 expression and developed immediately for EdU labeling. The sections were washed with PBS/3% BSA (wt/vol) followed by a 20-min incubation in PBS/0.5% Triton-X100 (vol/vol). The slices were again washed in PBS/3% BSA before EdU detection with the Click-iT EdU Alexa Fluor-555 Imaging kit (Invitrogen). Each slice was immersed in 120 μL of Click-iT developing mixture and incubated for 40 min at room temperature in the dark, according to the instructions of the manufacturer. Slices were washed once with PBS/3% BSA, twice with PBS and mounted under coverslips in fluorescence mounting medium (Fluoromount-G; Southern Biotech).

Microscopy and Cell Counts. With experimenters blinded to sample identity and condition, protein colocalization (multiple fluorochromes) was assessed in the confocal microscope. At least three mice were examined for each transgenic genotype. From each mouse, 30-μm coronal brain sections were immunolabeled to count $Olig2/EdU^+$ or $CC1/EdU^+$ double positive cells. All images were collected on an Olympus confocal microscope as *z*-stacks with 5-μm spacing, using standard excitation and emission filters for DAPI, FITC (Alexa Fluor-488), Texas Red (Alexa Fluor- 555), and Far Red (Alexa Fluor-647). For quantification, four or more low-magnification (20× objective) fields were collected per animal within each anatomical region of interest. Cells were viewed and counted using NIH ImageJ software (https://imagej.nih.gov/ij/).

Electron Microscopy. Four weeks after optogenetic stimulation (as above), mice were anesthetized with Euthasol and perfused with PB containing heparin followed by 2% paraformaldehyde (PFA; EMS), 2.5% glutaraldehyde (EMS), and 2 mM $CaCl_2$ in 0.1 M sodium cacodylate buffer, pH 7.4. After the brain was removed, a clean blade was used to resect a bilateral section containing either the anterior commissure or the corpus callosum below the ACC using an acrylic adult rodent brain matrix (World Precision Instruments). Following fixation overnight at 4 °C, the tissue was washed 3× for 10 min in 0.1 M sodium cacodylate buffer containing 2 mM CaCl2 at 4 °C. The samples were postfixed with 1% osmium tetroxide (EMS), 1.5% potassium ferrocyanide (EMS) in 0.1 M sodium cacodylate buffer for 1–2 h at 4 °C. They were washed three times with ultrafiltered water (EMS), and *en bloc*-stained with 2% uranyl acetate (EMS), for 1 h at 4 °C in the dark. Samples were washed twice with ultrafiltered water and allowed to equilibrate to room temperature. The samples were infiltrated and embedded in graded acetonitrile (50, 70, 90, and 100%) at room temperature according to the schedule of Edwards et al. (57). Samples were infiltrated with EMbed-812 resin (EMS) mixed 1:1 with acetonitrile for 1 h, followed by 1:1 EMbed-812:acetonitrile for 18 h. The samples were next placed into EMbed-812 for 3×1 h, then placed into silicone-embedding molds filled with fresh resin, which were then baked in a 60 °C oven for 48 h. Sections of 75- and 100-nm thickness were cut on a Reichert-Jung Ultracut E (Reichert-Jung) using a glass or an Ultra Diamond knife (EMS) and mounted on Formvar/carbon-coated slot grids (EMS) or 300-mesh Cu grids (EMS). Grids were contrast stained for 30 min in 2% uranyl acetate. Samples were imaged using an FEI Tecnai G2 Spirit TEM at 120 kV, and images were collected using an FEI Eagle 4k CCD camera at 16K magnification.

Statistics. We performed and analyzed all experiments blind to genotype and stimulation condition. Graphical data analyzed and presented using GraphPad Prism (v7). Group mean differences were analyzed using two-way ANOVA with Tukey or Tukey–Kramer post hoc tests to further examine pairwise differences for the EdU data. EM data were analyzed using a one-way ANOVA with Dunnett's test for multiple comparisons. In some instances, unpaired two-tailed Student's *t* tests were also reported. The relationship between behavioral data [from Weible et al. (27)] and g-ratio data were calculated using Kendall-τ b. Data are presented as mean $\pm$ SEM, unless otherwise indicated.

ACKNOWLEDGMENTS. We thank Prof. Yiyuan Tang (Texas Tech University) and Prof. Gary Lynch (University of California, Irvine) for their consultations on this work. We gratefully acknowledge the use of the electron microscopy facility at the Center for Advanced Materials Characterization in Oregon. This research was funded by Office of Naval Research Grants N00014-15-1-2148 and N00014-17-1-2824 (to the University of Oregon).

1. Blumenfeld-Katzir T, Pasternak O, Dagan M, Assaf Y (2011) Diffusion MRI of structural brain plasticity induced by a learning and memory task. *PLoS One* 6:e20678.
2. Wang S, Young KM (2014) White matter plasticity in adulthood. *Neuroscience* 276: 148–160.
3. Fields RD (2008) White matter in learning, cognition and psychiatric disorders. *Trends Neurosci* 31:361–370.
4. Tang Y-Y, Lu Q, Fan M, Yang Y, Posner MI (2012) Mechanisms of white matter changes induced by meditation. *Proc Natl Acad Sci USA* 109:10570–10574.
5. Tang Y-Y, et al. (2010) Short-term meditation induces white matter changes in the anterior cingulate. *Proc Natl Acad Sci USA* 107:15649–15652.
6. Tang Y-Y, et al. (2007) Short-term meditation training improves attention and self-regulation. *Proc Natl Acad Sci USA* 104:17152–17156.
7. Posner MI, Tang YY, Lynch G (2014) Mechanisms of white matter change induced by meditation training. *Front Psychol* 5:1220.
8. Xue SW, Tang YY, Tang R, Posner MI (2014) Short-term meditation induces changes in brain resting EEG theta networks. *Brain Cogn* 87:1–6.
9. Tang Y-Y, Hölzel BK, Posner MI (2016) Traits and states in mindfulness meditation. *Nat Rev Neurosci* 17:59.
10. Pizzagalli DA, Oakes TR, Davidson RJ (2003) Coupling of theta activity and glucose metabolism in the human rostral anterior cingulate cortex: An EEG/PET study of normal and depressed subjects. *Psychophysiology* 40:939–949.
11. Reinhart RMG (2017) Disruption and rescue of interareal theta phase coupling and adaptive behavior. *Proc Natl Acad Sci USA* 114:11542–11547.
12. Almeida RG, Lyons DA (2017) On myelinated axon plasticity and neuronal circuit formation and function. *J Neurosci* 37:10023–10034.
13. Fields RD (2015) A new mechanism of nervous system plasticity: Activity-dependent myelination. *Nat Rev Neurosci* 16:756–767.
14. Mount CW, Monje M (2017) Wrapped to adapt: Experience-dependent myelination. *Neuron* 95:743–756.
15. Barres BA, Raff MC (1993) Proliferation of oligodendrocyte precursor cells depends on electrical activity in axons. *Nature* 361:258–260.
16. Gibson EM, et al. (2014) Neuronal activity promotes oligodendrogenesis and adaptive myelination in the mammalian brain. *Science* 344:1252304.
17. Demerens C, et al. (1996) Induction of myelination in the central nervous system by electrical activity. *Proc Natl Acad Sci USA* 93:9887–9892.
18. Mensch S, et al. (2015) Synaptic vesicle release regulates myelin sheath number of individual oligodendrocytes in vivo. *Nat Neurosci* 18:628–630.
19. Makinodan M, Rosen KM, Ito S, Corfas G (2012) A critical period for social experience-dependent oligodendrocyte maturation and myelination. *Science* 337:1357–1360.
20. Sampaio-Baptista C, et al. (2013) Motor skill learning induces changes in white matter microstructure and myelination. *J Neurosci* 33:19499–19503.
21. McKenzie IA, et al. (2014) Motor skill learning requires active central myelination. *Science* 346:318–322.
22. Xiao L, et al. (2016) Rapid production of new oligodendrocytes is required in the earliest stages of motor-skill learning. *Nat Neurosci* 19:1210–1217.
23. Liu J, et al. (2012) Impaired adult myelination in the prefrontal cortex of socially isolated mice. *Nat Neurosci* 15:1621–1623.
24. Liu J, et al. (2016) Clemastine enhances myelination in the prefrontal cortex and rescues behavioral changes in socially isolated mice. *J Neurosci* 36:957–962.
25. Etxeberria A, et al. (2016) Dynamic modulation of myelination in response to visual stimuli alters optic nerve conduction velocity. *J Neurosci* 36:6937–6948.
26. Nagy B, Hovhannisyan A, Barzan R, Chen T-J, Kukley M (2017) Different patterns of neuronal activity trigger distinct responses of oligodendrocyte precursor cells in the corpus callosum. *PLoS Biol* 15:e2001993.
27. Weible AP, Piscopo DM, Rothbart MK, Posner MI, Niell CM (2017) Rhythmic brain stimulation reduces anxiety-related behavior in a mouse model based on meditation training. *Proc Natl Acad Sci USA* 114:2532–2537.
28. Hart PC, et al. (2010) Experimental models of anxiety for drug discovery and brain research. *Methods Mol Biol* 602:299–321.
29. Benninger Y, et al. (2006) Beta1-integrin signaling mediates premyelinating oligodendrocyte survival but is not required for CNS myelination and remyelination. *J Neurosci* 26:7665–7673.
30. Maldonado PP, Vélez-Fort M, Levavasseur F, Angulo MC (2013) Oligodendrocyte precursor cells are accurate sensors of local K+ in mature gray matter. *J Neurosci* 33: 2432–2442.
31. Sakry D, Yigit H, Dimou L, Trotter J (2015) Oligodendrocyte precursor cells synthesize neuromodulatory factors. *PLoS One* 10:e0127222.
32. Krasnow AM, Attwell D (2016) NMDA receptors: Power switches for oligodendrocytes. *Neuron* 91:3–5.
33. Saab AS, et al. (2016) Oligodendroglial NMDA receptors regulate glucose import and axonal energy metabolism. *Neuron* 91:119–132.
34. Trevisiol A, et al. (2017) Monitoring ATP dynamics in electrically active white matter tracts. *eLife* 6:e24241.
35. Miron VE, et al. (2013) M2 microglia and macrophages drive oligodendrocyte differentiation during CNS remyelination. *Nat Neurosci* 16:1211–1218.
36. Yuen TJ, et al. (2014) Oligodendrocyte-encoded HIF function couples postnatal myelination and white matter angiogenesis. *Cell* 158:383–396.
37. Watkins TA, Emery B, Mulinyawe S, Barres BA (2008) Distinct stages of myelination regulated by γ-secretase and astrocytes in a rapidly myelinating CNS coculture system. *Neuron* 60:555–569.
38. Ishibashi T, et al. (2006) Astrocytes promote myelination in response to electrical impulses. *Neuron* 49:823–832.
39. National Research Council (2011) *Guide for the Care and Use of Laboratory Animals* (National Academies Press, Washington, DC), 8th Ed.
40. Chomiak T, Hu B (2009) What is the optimal value of the g-ratio for myelinated fibers in the rat CNS? A theoretical approach. *PLoS One* 4:e7754.
41. Yeung MSY, et al. (2014) Dynamics of oligodendrocyte generation and myelination in the human brain. *Cell* 159:766–774.
42. Waxman SG, Bennett MV (1972) Relative conduction velocities of small myelinated and non-myelinated fibres in the central nervous system. *Nat New Biol* 238:217–219.
43. Waxman SG (1980) Determinants of conduction velocity in myelinated nerve fibers. *Muscle Nerve* 3:141–150.
44. Wu LMN, Williams A, Delaney A, Sherman DL, Brophy PJ (2012) Increasing internodal distance in myelinated nerves accelerates nerve conduction to a flat maximum. *Curr Biol* 22:1957–1961.
45. Ford MC, et al. (2015) Tuning of Ranvier node and internode properties in myelinated axons to adjust action potential timing. *Nat Commun* 6:8073.
46. Perge JA, Niven JE, Mugnaini E, Balasubramanian V, Sterling P (2012) Why do axons differ in caliber? *J Neurosci* 32:626–638.
47. Gong G, et al. (2009) Mapping anatomical connectivity patterns of human cerebral cortex using in vivo diffusion tensor imaging tractography. *Cereb Cortex* 19:524–536.
48. Raposo D, Sheppard JP, Schrater PR, Churchland AK (2012) Multisensory decision-making in rats and humans. *J Neurosci* 32:3726–3735.
49. Hu Y, et al. (2011) Somatosensory-evoked potentials as an indicator for the extent of ultrastructural damage of the spinal cord after chronic compressive injuries in a rat model. *Clin Neurophysiol* 122:1440–1447.
50. Keller TA, Just MA (2009) Altering cortical connectivity: Remediation-induced changes in the white matter of poor readers. *Neuron* 64:624–631.
51. Petersen SE, Posner MI (2012) The attention system of the human brain: 20 years after. *Annu Rev Neurosci* 35:73–89.
52. Etkin A, Büchel C, Gross JJ (2015) The neural bases of emotion regulation. *Nat Rev Neurosci* 16:693–700.
53. Kanske P, Heissler J, Schönfelder S, Bongers A, Wessa M (2011) How to regulate emotion? Neural networks for reappraisal and distraction. *Cereb Cortex* 21: 1379–1388.
54. Reis J, Fritsch B (2011) Modulation of motor performance and motor learning by transcranial direct current stimulation. *Curr Opin Neurol* 24:590–596.
55. Giordano J, et al. (2017) Mechanisms and effects of transcranial direct current stimulation. *Dose Response* 15:1559325816685467.
56. Reinhart RMG, Zhu J, Park S, Woodman GF (2015) Synchronizing theta oscillations with direct-current stimulation strengthens adaptive control in the human brain. *Proc Natl Acad Sci USA* 112:9448–9453.
57. Edwards HH, Yeh YY, Tarnowski BI, Schonbaum GR (1992) Acetonitrile as a substitute for ethanol/propylene oxide in tissue processing for transmission electron microscopy: Comparison of fine structure and lipid solubility in mouse liver, kidney, and intestine. *Microsc Res Tech* 21:39–50.
58. Traiffort E, Zakaria M, Laouarem Y, Ferent J (2016) Hedgehog: A key signaling in the development of the oligodendrocyte lineage. *J Dev Biol* 4:E28.